JACS
JOURNAL OF THE AMERICAN CHEMICAL SOCIETY

Article

pubs.acs.org/JACS

Intra- and Intermolecular Charge Transfer in Aggregates of Tetrathiafulvalene-Triphenylmethyl Radical Derivatives in Solution

Judith Guasch,[†,⊥] Luca Grisanti,[§,#] Manuel Souto,[†] Vega Lloveras,[†] José Vidal-Gancedo,[†] Imma Ratera,[†] Anna Painelli,[§] Concepció Rovira,[†] and Jaume Veciana*[,†]

[†]Institut de Ciència de Materials de Barcelona (ICMAB-CSIC)/CIBER-BBN, Campus Universitari de Bellaterra, E-08193 Cerdanyola del Vallès (Barcelona), Spain

[§]Dipartimento Chimica, GIAF, Parma University/INSTM-UdR, I-4310 Parma, Italy

Supporting Information

ABSTRACT: An extensive investigation of aggregation phenomena occurring in solution for a family of electron donor−acceptor derivatives, based on polychlorotriphenylmethyl radicals (PTM) linked via a vinylene-bridge to tetrathiafulvalene (TTF) units, is presented. A large set of temperature and/or concentration dependent optical absorption and electron spin resonance (ESR) spectra in a solution of dyads bearing different number of electrons and/or with a hydrogenated PTM residue offer reliable information on the formation of homo dimers and mixed valence dimers. The results shed light on the reciprocal influence of intramolecular electron transfer (IET) within a dyad and the intermolecular charge transfer (CT) occurring in a dimer between the TTF residues and are rationalized based on a theoretical model that describes both interactions.

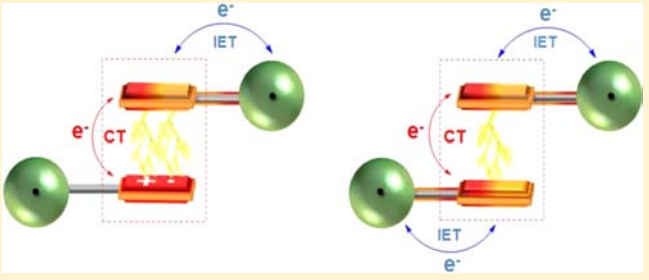

INTRODUCTION

The current interest on developing molecule-based spin-electronic devices such as switches, memories, or spin valves has stimulated the study of responsive bistable molecular materials with magnetic and/or conducting properties.[1−5] Organic electron donor−acceptor (D−A) dyads are excellent building blocks for bistable materials, due to their ability to switch between neutral and charge-separated states via an intramolecular electron transfer (IET) process in response to an external stimulus (temperature, pressure, light, solvent, magnetic and electrical fields).[6] Nonetheless, for most D−A dyads the absence of strong cooperative interactions makes the reverse IET process very fast, thus preventing a genuine bistability.[7−10] Cooperative and collective phenomena are driven in molecular aggregates by strong intermolecular interactions,[11,12] and therefore the design of new switchable D−A dyads with a propensity toward functional self-assembly is highly desirable. Tetrathiafulvalene (TTF) derivatives are excellent electron-donor molecules showing remarkable self-assembling phenomena both in solution and at solid state.[13−15] In fact, TTF derivatives are among the most widely utilized compounds for the development of organic metals,[16,17] where the self-assembly of neutral TTFs and their mono-oxidized cation-radicals ($TTF^{+\bullet}$) originate partially filled band structures and conductivity in solid state.[18] Likewise, $TTF^{+\bullet}$ molecules self-assemble in solid state leading to Mott insulators and diamagnetic solids. Recently, Kochi and Rosokha presented a very detailed study of the self-assembly of unsubstituted TTFs in solution.[19] They unequivocally established the thermodynamic framework for aggregation, shedding light on the self-assembly of this important family of compounds in solution.

In this article we analyze the TTF-driven supramolecular aggregation of a recently reported organic D−A dyad **1**, formed by a TTF unit, which acts as the electron-donor, conjugated through a vinylene bridge to a polychlorotriphenylmethyl radical (PTM) that acts as an acceptor. Dyad **1** can be found in two stable states in solution, the neutral **1a** and the zwitterionic **1b** states, depicted in Scheme 1, whose relative concentration can be modified by moderate changes in the molecular

Scheme 1. Neutral 1a and Zwitterionic 1b States of Dyad 1[a]

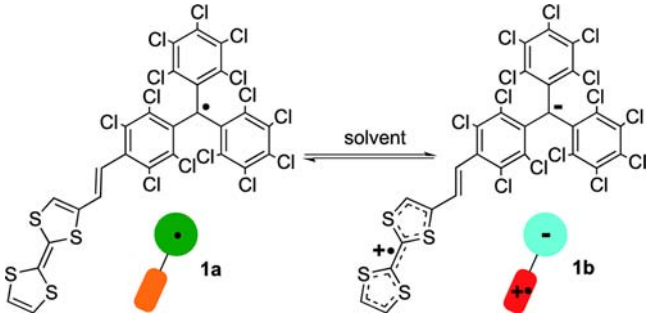

[a]The two states are interchanged by an IET process between the TTF and the PTM subunits.

Received: January 10, 2013
Published: March 21, 2013

   dx.doi.org/10.1021/ja400281b | J. Am. Chem. Soc. 2013, 135, 6958−6967

environment and solvent polarity.[20] Particularly remarkable is the observation that the positive charge introduced on the TTF unit by the IET process favors the TTF-based self-assembly of dyad **1** in solution.[20]

To better understand the subtle interplay between intramolecular ET and the intermolecular charge transfer (CT) processes in aggregates based on dyad **1**, we undertook an extensive investigation of several precursors and derivatives of this dyad, compounds **2**−**5** (Scheme 2), based on the collection

Scheme 2. Derivatives and Precursors of Dyad 1

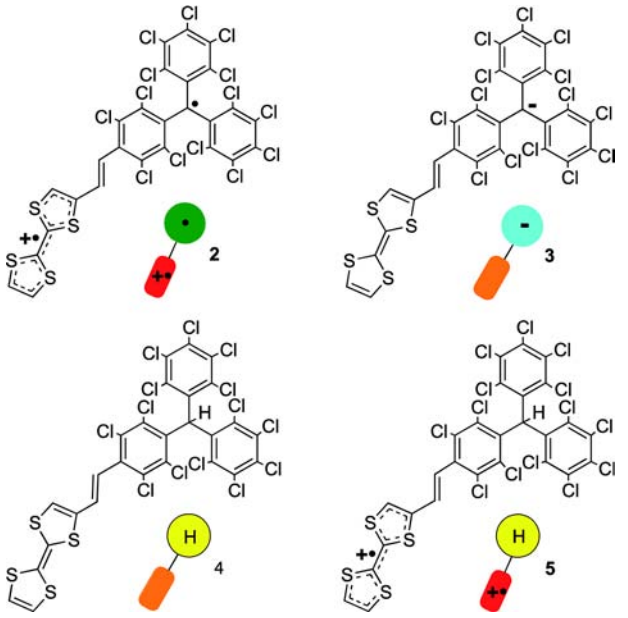

of electrochemical data, UV/vis/NIR and electron spin resonance (ESR) spectra as a function of temperature and/or concentration. First, we analyzed the self-aggregation of salt **2**, which contains the TTF unit oxidized as $TTF^{+\bullet}$ (Scheme 3; Eq. 1), and then we focused on how this cation-radical aggregates with dyad **1** (Scheme 3; Eqs. 2 and 3). To gain a deeper insight into the complex physics governing aggregation in these systems, we also present an extensive study of aggregation in protonated-PTM compounds **4** and **5**. In this study, following the same lines proposed by Kochi et al.[19] on unsubstituted

Scheme 3. Dimerization Processes of Salt 2 to Form the Homo Dimer 2·2, (Eq. 1); of 1a and 2 to Produce the Mixed-Valence (MV) Dimer 1a·2 (Eq. 2); and of 1b and 2 to Give the MV Dimer 1b·2 (Eq. 3)

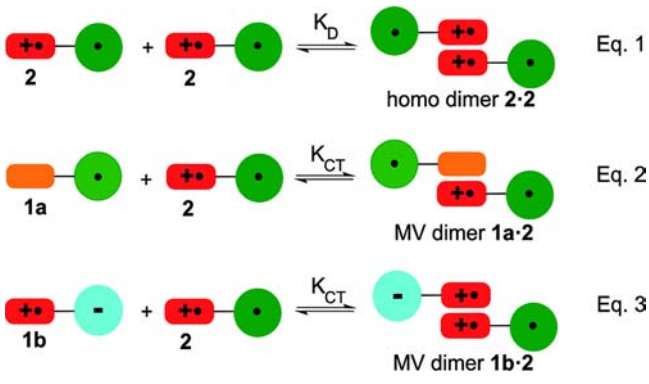

TTFs, we describe the dimerization processes shown in Scheme 4, Eqs. 4 and 5, that imply intermolecular CT processes, while

Scheme 4. Dimerization Processes of Salt 5 to Form the Homo Dimer 5·5 (Eq. 4) and of 5 and 4 to Produce the MV Dimer 4·5 (Eq. 5)

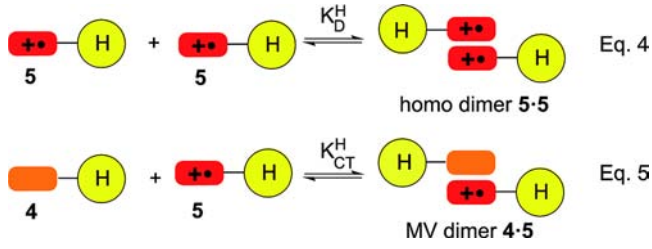

the IET process is suppressed since the protonated-PTM unit is not a good electron acceptor. Compounds **4** and **5** are therefore useful simplified models to study the TTF-based equilibria of **1** and **2**, which facilitate the determination of the role of the IET process of dyad **1** in its aggregation phenomena.

Based on this extensive experimental analysis, a new model is proposed that, merging a Hubbard-like description of the intermolecular CT interaction with an essential-state description of the IET, rationalizes the complex spectroscopic behavior of homo and mixed-valence (MV) dimers based on compounds **1**−**5**. In summary, the supramolecular properties of dyad **1** and its derivatives, which have a bulky paramagnetic group attached to the TTF core, are based on the interplay between IET and intermolecular CT processes. The understanding of this dynamic system is crucial to control its multifunctionality and to fully exploit its potential for applications in the field of molecular electronics and spintronics.[5,21−24]

RESULTS AND DISCUSSION

1. Synthesis. *1.1. Synthesis of Compounds 1, 3, and 4.* Compounds **1**, **3**, and **4** were prepared as previously reported.[20] Compound **4** was obtained through a Horner-Wadsworth-Emmons reaction of a protonated PTM derivative functionalized with a phosphonate group[25] and 2-formyltetrathiafulvalene.[26] Subsequent deprotonation with potassium hydroxide of **4** gave the PTM anion derivative **3** which was stabilized using 18-Crown-6 to complex the K^+ counterion. Oxidation of **3** with silver nitrate afforded dyad **1**, which is stable under atmospheric conditions.

1.2. Synthesis of Salts 2 and 5. The synthetic procedures for the preparation of the hexafluoroantimoniate salts **2** and **5** are described in detail in the Supporting Information. In brief, stoichiometric quantities of $NOSbF_6$ were used to oxidize the TTF subunits of **1** and **4** under inert conditions at r.t. in freshly distilled CH_2Cl_2. Salts **2** and **5** were obtained as microcrystalline dark brown solids with almost quantitative yields.

2. Electrochemical Generation and Characterization. Cyclic voltammetries (CV) of compounds **1**, **3**, and **4** were performed in CH_2Cl_2 under an inert atmosphere of argon at r.t. using *n*-Bu_4NPF_6 as electrolyte (0.15 M). Voltammograms in Figure 1 show two or three quasi-reversible redox waves in accordance with the number of electroactive units of the molecules. Specifically, compound **4** shows two redox waves due to the oxidation of the TTF unit to $TTF^{+\bullet}$ and TTF^{2+} with redox potentials of $E_{1/2}^{ox1}$ = +0.448 V and $E_{1/2}^{ox2}$ = +0.965 V, versus Ag/AgCl, respectively (Figure 1, blue line). The voltammogram of salt **3** shows three waves related to the

dx.doi.org/10.1021/ja400281b | J. Am. Chem. Soc. 2013, 135, 6958−6967

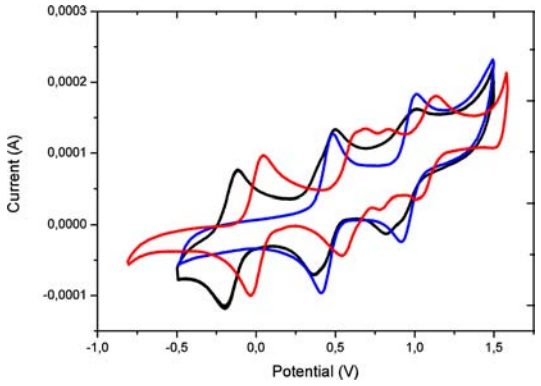

Figure 1. Cyclic voltammetry of dyad **1** (red line) and compounds **3** (black line) and **4** (blue line) in CH_2Cl_2 using n-Bu_4NPF_6 as electrolyte at r.t. The potentials are referred to Ag/AgCl.

following redox pairs: $PTM^-/PTM^\bullet$, $TTF/TTF^{+}\cdot$, and $TTF^{+}\cdot/TTF^{2+}$ with redox potentials of $E_{1/2}^{red} = -0.156$ V, $E_{1/2}^{ox1} = +0.434$ V, and $E_{1/2}^{ox2} = +0.916$ V versus Ag/AgCl (Figure 1, black line). Interestingly, the CV of dyad **1** exhibits a shift of $PTM^-/PTM^\bullet$, $TTF/TTF^{+}\cdot$, and $TTF^{+}\cdot/TTF^{2+}$ waves toward higher potentials in comparison with **3** and **4**. The shift for the PTM unit is due to the initial charge and counterion ([18-C-6]K^+) of anion **3** with respect to the radical **1**. To our surprise, the first oxidation wave of the TTF for **1** is splitted into two redox waves. It has been reported that when two or more moieties of TTF are sufficiently close to each other, the first oxidation wave to the radical cation splits in two steps.[27] This suggests an electronic stabilization of the first-formed radical cation $\mathbf{1}^{+\bullet}$ by the π electrons of a second **1** dyad forming mixed-valence (MV) dimers $(TTF)_2^{+}\cdot$.[27] On the other hand, the reversible second oxidation step of the TTF unit leading to the formation of dications indicates that the two molecules are at larger distance and no longer in electronic communication.

Due to the good separation of the redox waves of the studied compounds, some species can be generated in chronoamperometric experiments, setting the proper redox potentials. This possibility was particularly useful for species **1** and **2**, which are very stable in the electrolyte solution, to avoid problems related to their limited solubility and tendency of precipitation in other environments, as commented in sections 4 and 5.

3. Homo Dimers of Salts 2 and 5. We start the discussion with the analysis of dimerization equilibria of salts **2** and **5** (see Eq. 1 and Eq. 4), studied by means of ESR and UV/vis/NIR spectra collected at variable temperature and different concentrations.

3.1. ESR Spectroscopic Measurements. ESR spectra of salts **2** and **5** in CH_2Cl_2 solutions (0.05 mM) were measured at different temperatures. At 300 K both spectra show complex signals whose symmetric shapes confirm the high purity of the two compounds. Specifically, the ESR signal of salt **5** at 300 K consists of eight overlapped lines centered at $g = 2.0074$ (Figure 2) due to the coupling of the unpaired electron of the $TTF^{+}\cdot$ subunit with the three protons (H^a, H^b, and H^c) of the same subunit and the two vinylene protons (H^d and H^e) of the bridge (see Figure 2a). This 8-line signal can be simulated (Figure 2b) with the coupling of the two protons H^a and H^b, which appear as equivalent with a hyperfine coupling constant $a_H = 1.24$ G, a third proton H^c with $a_H = 1.05$ G, the nearest vinylene proton H^d with $a_H = 0.59$ G, and the furthest vinylene proton H^e with $a_H = 0.18$ G. Both the g-value and estimated

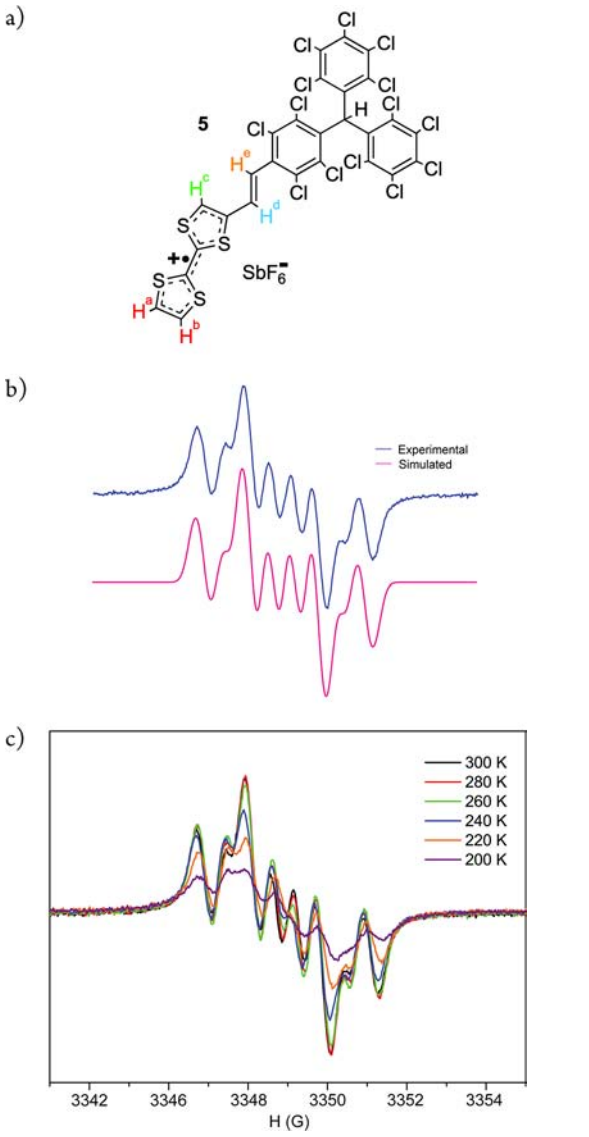

Figure 2. (a) Structure of salt **5** showing the H nuclei responsible of the hyperfine splitting. (b) Experimental (blue line) and simulated (pink line) spectra in CH_2Cl_2 at 300 K with the coupling constants given in Table 1. (c) Experimental ESR spectra of salt **5** performed in CH_2Cl_2 in the temperature range of 200−300 K.

hyperfine coupling constants are well in line with the typical values for monosubstituted $TTF^{+}\cdot$ derivatives.[15,28−32] On this basis we safely conclude that salt **5** exists in CH_2Cl_2 solution at 300 K as free species, not undergoing aggregation.

When temperature is lowered, the line width of the ESR peaks progressively increases while the total intensity of the signal decreases, to disappear completely at 160 K. These changes are fully reversible with temperature. This complex behavior suggests the presence of a dimerization equilibrium between the paramagnetic monomer **5** and the diamagnetic homo dimer **5**·**5** (Scheme 4; Eq. 4), shifted toward the dimer at low temperature. Similar results were obtained for salt **2** as shown in Figure 3 and Table 1.

The ESR spectrum of salt **2** at 300 K consists of two groups of lines centered at the g-values of 2.0076 and 2.0025. These are the typical g-values exhibited by open-shell species containing $TTF^{+}\cdot$ and PTM units, respectively. The hyperfine splitting observed for the group of lines centered at 2.0076 can be

dx.doi.org/10.1021/ja400281b | J. Am. Chem. Soc. 2013, 135, 6958−6967

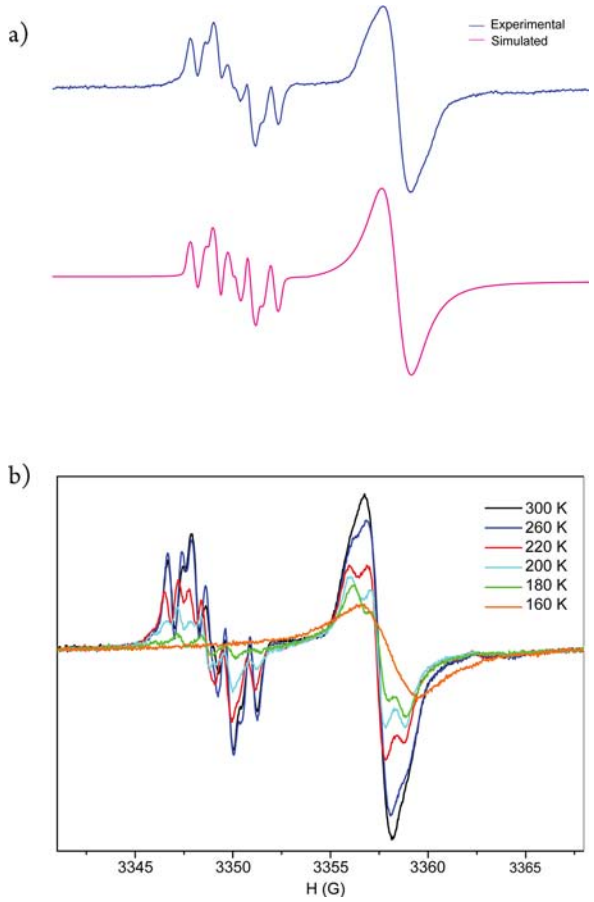

Figure 3. (a) Experimental (blue line) and simulated (pink line) spectra of salt **2** at 300 K with the coupling constants given in Table 1. (b) Experimental ESR spectra of salt **2** performed in CH_2Cl_2 in the temperature range of 160−300 K.

simulated with hyperfine coupling constants (see Table 1) very similar to those determined for **5**, whereas the group of lines corresponding to the radical residing on the PTM subunit appears unresolved. We conclude that salt **2** in CH_2Cl_2 at 300 K does not dimerize and behaves as a biradical species with two nonmagnetically coupled open-shell subunits.

When temperature is lowered, the lines associated with both TTF and PTM subunits decrease in intensity while the signal related to the PTM subunit becomes more resolved. At 220 K, the PTM signal appears as three overlapped lines, which can be simulated with the coupling of the unpaired electron with two equivalent protons with a_H = 1.01 G. The PTM signals are very similar to those collected for PTM diradicals linked by *p*-phenylenevinylene bridges, where the two PTM species are magnetically interacting and coupled with the two closest vinylene protons, and are safely ascribed to the presence of the homo dimer **2·2**.[33] Below 160 K, the signal corresponding to the TTF subunit disappears completely while the PTM signal appears as a single broad line without a resolved hyperfine structure. This effect and the improved resolution of the signal of the PTM subunit in the temperature range of 300−160 K are well-known for PTM radicals and are ascribed to the slowing down of the tumbling of these large groups when temperature is decreased. These temperature-induced changes are completely reversible and fully consistent with the dimerization of **2** at low temperature. The intensity of the ESR signal decreases with decreasing temperature (see Figure S4), suggesting that in the homo dimer **2·2** the two $TTF^{+}\cdot$ subunits are magnetically coupled in a singlet (ESR-silent) ground state and in addition they are able to transmit an antiferromagnetic interaction between the two unpaired spins of the PTM subunits. Temperature-dependent ESR spectra of **2** and **5** can be analyzed to obtain quantitative information about the dimerization processes in Eqs. 1 and 4, and in particular to extract the relevant thermodynamic parameters ΔH and ΔS and equilibrium constants K_D, as discussed in the SI. The analysis was performed on solutions with different concentrations (see SI) leading to the results summarized in Table 2.

Table 2. Equilibrium Constants and Thermodynamic Parameters of the Dimerization Processes of Salts 2, 5, and Unsubstituted $TTF^{+}\cdot$ at 298 and 180 K Obtained through ESR Spectroscopy

homo dimer	ΔS (eu)	ΔH (kcal·mol^{-1})	K_D (at 298 K)	K_D (at 180 K)
2·2	−17	−6.2	8.76	8.44×10^3
5·5	−31	−8.8	0.56	9.25×10^3
$TTF^{+}\cdot/TTF^{+}\cdot$[a]	−18	−3.8	0.07	4.79

[a]Thermodynamic values and equilibrium constants of $TTF^{+}\cdot CB^{-}$ (CB^{-}: *closo*-dodecamethylcarboranate) obtained in CH_2Cl_2 from ref 19.

The equilibrium constants for the dimerization of salts **2** and **5** have similar magnitudes and are much larger than those obtained for unsubstituted $TTF^{+}\cdot$ radicals.[19] Apparently, the large PTM subunit attached to the TTF moiety, rather than preventing the aggregation processes due to a hypothetical steric hindrance, favors the aggregation by keeping the two TTF subunits together in a "cage-like" structure.

3.2. UV/vis/NIR Spectroscopic Measurements. Additional information on the dimerization in solution of **2** and **5** is obtained from optical absorption spectra. Due to overshadows and saturation problems at high energies caused by the very intense absorption of the PTM units, we only focused in the near-IR spectral region where homo dimers of the $TTF^{+}\cdot$ radical show a characteristic absorption band around 750 nm (13 300 cm^{-1}).[15,19,27,34−39] Relevant spectra, measured in CH_2Cl_2, are shown in Figure 4.

Table 1. ESR Data for Monomeric Salts 2 and 5 at 300 K and Homo Dimer 2·2 at 180 K

species	paramagnetic subunit[a]	T (K)	g-value	$a_H^{a/b}$ (G)	a_H^{c} (G)	a_H^{d} (G)	a_H^{e} (G)	$\Delta H_{1/2}$
5	TTF	300	2.0074	1.24[b]	1.05	0.59	0.18	0.30
2	TTF	300	2.0076	1.24[b]	1.00	0.62	0.18	0.22
	PTM	300	2.0025	-	-	-	-	1.44
homo dimer **2·2**	PTM	180	2.0027		-	-	1.01[d]	1.00[c]

[a]Paramagnetic subunits responsible of the observed ESR signals. [b]The two protons H^a and H^b present the same coupling constant. [c]Obtained at 200 K. [d]Coupling with two H^e protons of the two interacting molecules.

dx.doi.org/10.1021/ja400281b | J. Am. Chem. Soc. 2013, 135, 6958−6967

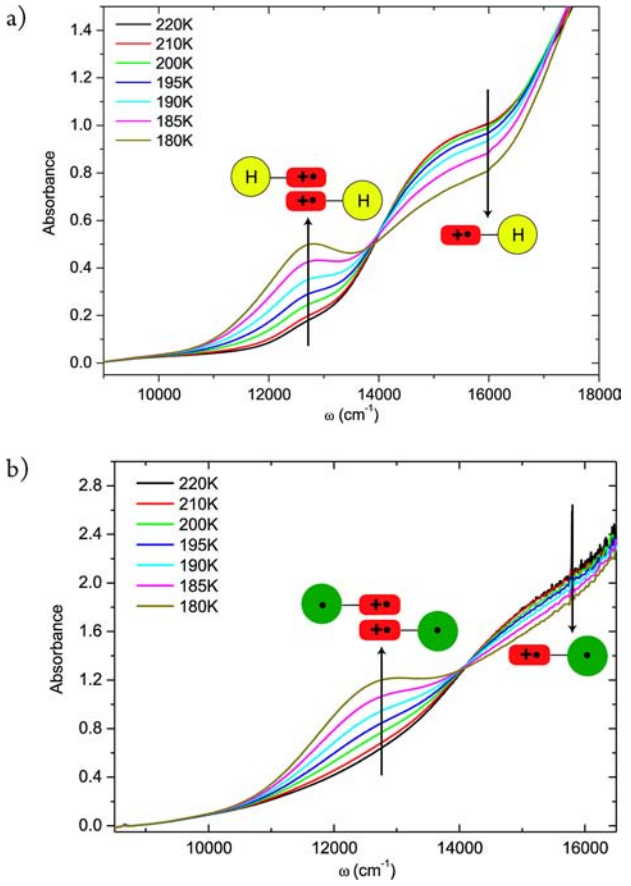

Figure 4. T-dependent UV/vis/NIR of a solution of salts (a) **5** (2.88 mM) and (b) **2** (1.12 mM) in CH_2Cl_2.

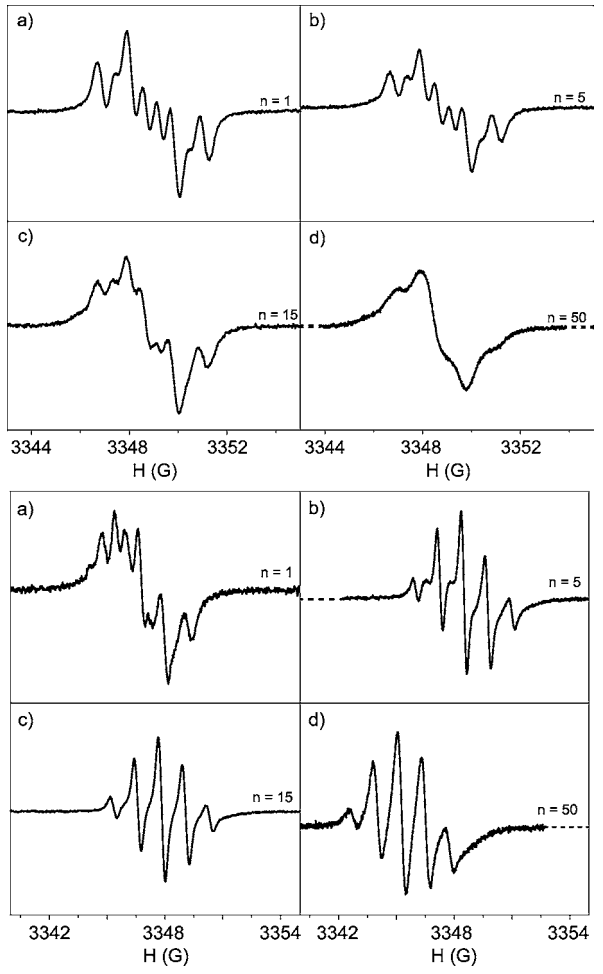

Figure 5. ESR spectra of 1:*n* mixtures of **5** and **4** in CH_2Cl_2 with n = 1 (a); n = 5 (b); n = 15 (c); and n = 50 (d). Top box shows spectra at 300 K and bottom box at 200 K.

Upon lowering the temperature, spectra collected for solutions of salts **2** and **5** show a progressive increase of a broad band located around 780 nm (12 800 cm^{-1}). This band, ascribed to the charge-resonance between $TTF^{+\bullet}$ species, is a clear signature of the formation of the homo dimers. Concomitantly, the monomer band centered around 650 nm (15 385 cm^{-1}) shows a progressive decrease of intensity. These bands strongly overlap with the red tail of a very intense PTM based monomer band, hindering a reliable spectral deconvolution and hence the quantitative analysis of optical spectra for the estimate of equilibrium constants.

4. Mixed-Valence Dimers 1·2 and 4·5. The capacity of $TTF^{+\bullet}$ to associate with its neutral precursor TTF to form mixed-valence dimers has been widely reported both in solution and in solid state.[5,16,40] This cross-association is stabilized by charge-resonance (delocalization) between the two TTF units.[19,35,37,41−43] In this section the formation of mixed-valence dimers obtained by the cross-association of **1** with **2** and of **4** with **5** (Eqs. 2 and 5) is studied by temperature-dependent ESR and NIR spectra.

4.1. ESR Spectroscopic Measurements. ESR spectra were measured for a 0.05 mM solution of salt **5** in CH_2Cl_2 upon adding increasing amounts of **4** (n = 1, 5, 15, and 50 equiv, Figure 5) at 300 and 200 K.

The ESR spectrum measured at 300 K after adding 1 equiv of **4** to a solution of salt **5** shows a symmetric 8-line signal centered at g = 2.0083 and assigned to the $TTF^{+\bullet}$ subunit. This spectrum, practically identical to that obtained from the pure solution of salt **5**, indicates negligible association in these conditions. Although the ESR spectrum obtained after adding 5 equiv of **4** to the solution of **5** shows a slight asymmetry of the signal, suggesting the presence of both monomers and MV dimers, the addition of 15 equiv of **4** was needed to obtain a clear asymmetric spectrum indicative of the presence of two ESR active species with different g-values. The spectrum obtained in these conditions can be safely decomposed as the sum of two spectra: the monomeric 8-line signal of **5** and a 5-line signal corresponding to the MV dimer **4·5** (Table 3).

The MV dimer signal (Figure 5; bottom) was clearly identified in low-temperature spectra, where the dimerization process is almost completely shifted toward the MV dimer species. The 5-line signal of the MV dimer **4·5** can be simulated accounting for the hyperfine coupling of the unpaired electron with four quasi-equivalent protons with a_H = 1.25 G related to the pair of interacting $TTF/TTF^{+\bullet}$ units (Figure 6).

We assign the four quasi-equivalent protons to H^a and H^b of the two interacting $TTF/TTF^{+\bullet}$ subunits that share the unpaired electron in agreement with the theoretical model presented in section 5. We cannot however fully exclude that the exchange dynamics of the unpaired electron between the two TTF moieties is slow in comparison with the ESR time scale and that the four protons (H^a, H^b, H^c, and H^d) belong to a single TTF subunit with a different conformation than the monomer due to the dimerization process.

dx.doi.org/10.1021/ja400281b | J. Am. Chem. Soc. 2013, 135, 6958−6967

Table 3. Summary of the ESR Spectral Data for Neutral MV Dimer Species Formed by Compounds 1, 2, 4, and 5 in CH_2Cl_2

species	paramagnetic subunit[a]	g-value	$a_H^{a/b}$ (G)	a_H^{c} (G)	a_H^{d} (G)	a_H^{e} (G)	$\Delta H_{1/2}$
Monomer **5**[b]	TTF	2.0074	1.24	1.05	0.59	0.18	0.30
MV dimer **4·5**[d]	TTF	2.0083	1.25[c]	-	-	-	0.32
Monomer **2**[b]	TTF	2.0076	1.24	1.00	0.62	0.18	0.22
	PTM	2.0025	[f]	-	-	-	1.44
Monomer **1**[b]	PTM	2.0032	1.60	-	-	-	1.55
MV dimer **1·2**[e]	TTF	2.0082	1.25[c]	-	-	-	0.25
	PTM	2.0029		-	-	1.10[g]	1.00

[a]Paramagnetic subunits responsible of the observed ESR signals. [b]Spectral data at 300 K. [c]Four protons present the same coupling constant. [d]Spectra data of a mixture of **4** and **5** (0.75 mM:0.05 mM) at 200 K. [e]Spectral data of a mixture of **1** and **2** (0.05 mM:0.05 mM) at 200 K. [f]Coupling constant not determined due to dimeric interferences. [g]Coupling with two H^e protons of the two interacting molecules.

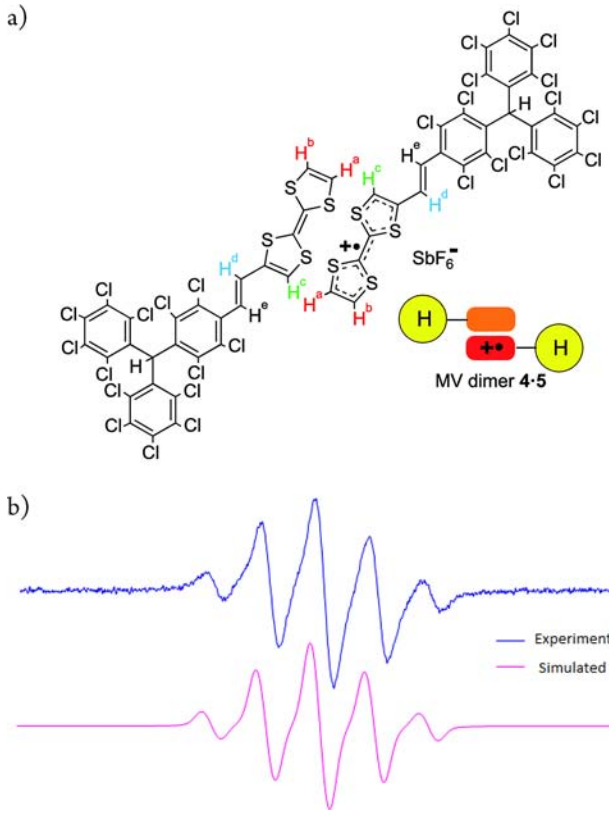

Figure 6. (a) Structure of the MV dimer **4·5** showing the protons that might be responsible for the hyperfine coupling. (b) Experimental (blue line) and simulated (pink line) ESR spectra of the MV dimer **4·5** obtained from a solution of **5** and **4** (0.05 mM:0.75 mM) at 200 K in CH_2Cl_2.

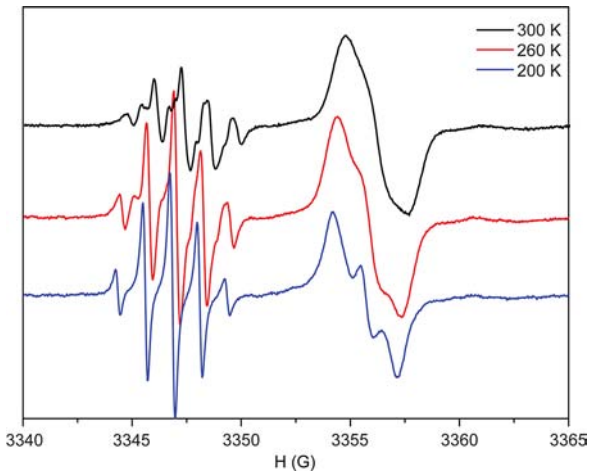

Figure 7. T-dependent ESR spectra in CH_2Cl_2 of a 1:1 nominal mixture of **1** and **2** electrochemically obtained after oxidizing the precursor **3** at 300 K (black line), 260 K (red line), and 200 K (blue line).

Having established the formation of the MV dimer **4·5** by ESR measurements, similar experiments were run on their radical counterparts, dyad **1** and salt **2**. As mentioned in section 2, we use chronoamperometry to produce equimolar mixtures of **1** and **2**. Thus, a solution of the anion precursor **3** in CH_2Cl_2 was electrochemically oxidized with a potential of +0.7 V and the current needed to obtain a nominal 1:1 mixture of dyad **1** and salt **2** (nominal 1.5 e^-). Temperature-dependent ESR spectra of the resulting solution are shown in Figure 7 and relevant data are listed in Table 3.

At 300 K the spectrum contains two signals at g = 2.0082 and g = 2.0029 ascribed to the $TTF^{+\bullet}$ and PTM subunits, respectively. The shape of the signal centered at 2.0082 reveals that the mixture contains the MV dimer **1·2** (5-line signal), although some amounts of the monomeric species **2** (8-line signal) are also present. Accordingly, the PTM signal at g = 2.0029 appears as a broad line, as expected for dimeric species (3-line signal) with some residual amounts of monomers **1** (1-line signal) and **2** (1-line signal).[33] At low temperatures, the 5-line signal of the TTF subunit, ascribed to the MV dimer **1·2**, becomes dominant over the 8-line signal of monomer **2**. As discussed above, the 5-line signal of the mixed dimer can be modeled accounting for the coupling of the unpaired electron residing on the $TTF/TTF^{+\bullet}$ subunits with four equivalent protons with a_H = 1.25 G, which probably correspond to the protons H^a and H^b of the two molecules. Similarly, the PTM signal becomes a well resolved 3-line signal, which in analogy with the homo dimer **2·2**, can be explained by the fact that each of the two spins of the PTM subunits of a MV dimer **1·2** interact with its closest proton and the same proton of the second molecule with a coupling constant of a_H = 1.10 G. An antiferromagnetic interaction between PTM subunits through the TTF-dimer bridge is also suggested in this case due to the decrease of the intensity of the PTM signal when the temperature is lowered (Figure S5). Moreover, the relative intensity of TTF and PTM signals was also used to study the importance of the IET in the MV dimer. Specifically, the (double integrated) areas of the signals ascribed to the TTF and PTM subunits (Figure S5) suggest a ratio of TTF versus PTM spin density of 0.38 at 300 K further decreasing toward 0.2 at 180 K. These numbers are significantly lower than the theoretical 0.5 value expected for an equimolar mixture of **1** and **2**, and for the corresponding hypothetical MV dimer **1a·2** with

dx.doi.org/10.1021/ja400281b | J. Am. Chem. Soc. 2013, 135, 6958−6967

frozen IET. While we cannot fully exclude the presence in solution of the homo dimer **2**·**2**, whose TTF subunit is ESR silent, we believe that the nonstoichiometric ratio of TTF and PTM spin densities is due to the IET process of **1** that, together with the CT, drives electron-delocalization in the whole structure. A detailed model for this intriguing phenomenon is presented in section 5; here we just indicate that ESR spectra suggest a finite weight in the ground state of species that can be described as MV dimer **1b**·**2** with a silent $(TTF^{+}\cdot)_2$ subunit.

The electron-delocalization driven by the interplay of IET and CT is responsible for fractional charges and fractional (nonstoichiometric) spin-densities. The subtle interplay between the two driving forces leads to a delicate balance that is strongly affected by environmental interactions. Quite interestingly, solutions of **1**·**2** dimers obtained by mixing chemically isolated dyad **1** and salt **2** have distinctively different ESR and optical spectra than measured for electrochemically prepared species (see Supporting Information). Specifically, ESR spectra obtained from dimers formed by chemically isolated **1** and **2** show at all temperatures a lower proportion of $TTF^{+}\cdot$ compared to the results shown in Figure 7 for electrochemically prepared species, and the ratio of $TTF^{+}\cdot$ versus PTM spin density of 0.38 at 300 K obtained in the electrochemical experiments is reduced here to 0.10. Such a change is most probably due to the large difference in the ionic strengths existing in the media used in the two preparation methods. Indeed, the addition of electrolyte to a solution of chemically prepared dimers increases the ratio of $TTF^{+}\cdot$ versus PTM spin density achieving values similar to those obtained in the electrochemical method.

4.2. NIR Spectroscopic Measurements. It is well-known that TTF-$TTF^{+}\cdot$ MV dimers show a CT absorption band in the NIR region and more specifically around 5000−6000 cm^{-1}. Therefore, we measured T-dependent absorption NIR spectra of mixtures of **4** and **5** as well as **1** and **2** in CH_2Cl_2 solutions. Specifically, 5 (Figure S3) and 10 equiv (Figure 8) of **4** were added to a 0.07 mM solution of **5** in CH_2Cl_2 in order to promote the formation of the MV dimer **4**·**5**.

Although separate solutions of **4** and its chemically oxidized salt **5** do not show, even at high concentrations and very low temperatures, any electronic transition in the 1000−3000 nm (3300−10 000 cm^{-1}) range, mixtures of **4** and **5** exhibit a broad band centered at 1840 nm (5450 cm^{-1}) whose intensity increases upon lowering temperature. This band is safely assigned to the intermolecular electron transfer process between the neutral TTF and the $TTF^{+}\cdot$ subunits of the MV dimer **4**·**5**.[19,35,44−47]

Figure 9 shows the temperature dependent absorption spectra of a nominal 1:1 mixture of **1** and **2**, generated by a chemical oxidation (with 1.5 equiv of $NOSbF_6$) of precursor **3** dissolved in CH_2Cl_2 (0.10 mM).

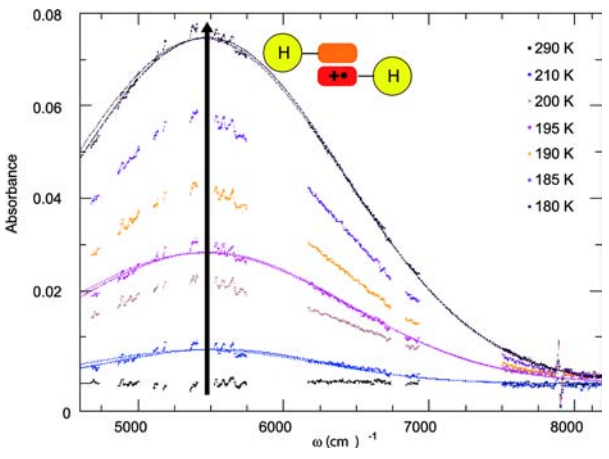

Figure 8. T-dependent NIR spectra (broken lines: experimental spectra; solid and dotted lines: fittings) of a 10:1 mixture of **4** and salt **5** in CH_2Cl_2 in the temperature range of 180−290 K.

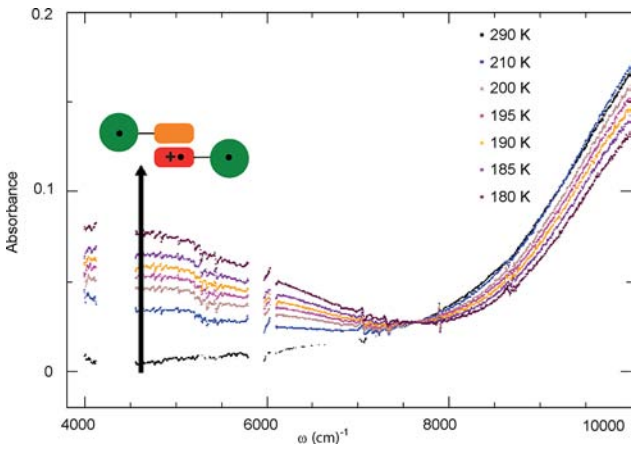

Figure 9. T-dependent NIR spectra of a mixture of dyad **1** and salt **2** (1:1) obtained by a chemical oxidation of **3** with $NOSbF_6$ (1.5 equiv) in CH_2Cl_2 in the temperature range of 180−290 K.

These spectra also show a broad band in the NIR region whose intensity increases when the temperature is lowered. This band is a clear signature of the electron transfer process between the neutral TTF and the cation-radical $TTF^{+}\cdot$ subunits of the MV dimer **1**·**2**.[19,35,44−47] Interestingly, this very broad band occurs at an energy (4170 cm^{-1}, or 2398 nm), lower than that of the protonated derivatives (5450 cm^{-1}) pointing to the nontrivial role played by IET processes in this system. The IET only marginally affects the intermolecular charge transfer process in the **2**·**2** homo dimer whose CT band occurs at very similar frequencies as for **5**·**5** (see Figure 4). On the opposite, in the MV dimer **1**·**2**, IET processes are responsible for a partial delocalization of the electrons on the PTM subunits leading to a lowering of relevant absorption frequencies. Since in MV dimers **1**·**2** and **4**·**5** the CT bands are well isolated and not superimposed to other bands, it is possible to extract information on relevant equilibrium constants from the temperature evolution of their intensities. The analysis is described in the Supporting Information. Relevant results are collected in Table 4, and are compared with the equilibrium constants estimated for the MV dimers based on unsubstituted TTF species (from ref 19). The equilibrium

Table 4. Equilibrium Constants and Thermodynamic Parameters of the Cross-Association Processes of 4/5, 1a/2, and TTF/$TTF^{+}\cdot$ at 298 K and 180 K Obtained through Absorption Spectroscopy

MV dimer	ΔS (eu)	ΔH (kcal·mol^{-1})	K_{CT} (298 K)	K_{CT} (180 K)
1·**2**	−28	−8.6	1.95	2.80×10^4
4·**5**	−24	−7.0	0.80	1.86×10^3
TTF/$TTF^{+}\cdot$[a]	−16	−5.5	3.44	1.52×10^3

[a]From ref 19.

dx.doi.org/10.1021/ja400281b | J. Am. Chem. Soc. 2013, 135, 6958−6967

constants are much smaller at 298 K than at 180 K, and are similar for the three systems, even if at low temperatures, the MV dimer **1·2** shows an equilibrium constant more than 1 order of magnitude higher than the other dimers. It is suggestive to ascribe this increased stability to the contribution of the intramolecular electron transfer that delocalizes the electrons along the vinylene bridge and the PTM subunit. As discussed above, the delocalization is strongly affected by the interaction with the environment and, much as ESR spectra, NIR spectra of chemically prepared **1·2** dimers differ from those of electrochemically prepared species. As will be discussed in section 5, this can be ascribed to the stabilization of charge-separated structures in chemically prepared solutions.

5. Intermolecular CT and IET: a Model. To provide a simple and comprehensive picture of CT processes in TTF-PTM dyads, we propose a model that combines the Hubbard model, representing the standard model for TTF-based dimers,[48] with essential state models for D−A dyads.[8,10,12]

As mentioned before, the hydrogenated PTM subunits of compounds **4** and **5** do not act as electron acceptor, so that IET is suppressed. The **5·5** and **4·5** dimers then represent a useful starting point to discuss intermolecular CT in the absence of IET, allowing for the definition and parametrization of the relevant Hubbard model. Specifically, both dimers can be described based on the following two-site Hubbard model:[48]

$$H = -t \sum_{\sigma=\alpha,\beta} (a^{\dagger}_{1\sigma}a_{2\sigma} + a^{\dagger}_{2\sigma}a_{1\sigma}) + U(n_{1\alpha}n_{1\beta} + n_{2\alpha}n_{2\beta})$$

where $a^{\dagger}_{i\sigma}$, $a_{i\sigma}$ are the creation and annihilation operators, respectively, of an electron with spin σ on the frontier orbital (the HOMO) of one of the two TTF sites, and $n_{i\sigma}$ counts the number of electrons with spin σ on the ith site. A pictorial representation of relevant parameters is shown in the top panel of Figure 10. The hopping integral, t, is responsible for the electronic delocalization between the two TTF-sites, and U measures the repulsion between two electrons residing on the same orbital. The homo dimer **5·5** has two electrons and the MV dimer **4·5** has three electrons. The charge-resonance shows up with so-called charge-transfer bands in the NIR, a well-known result for TTF-dimers.[48] Specifically, setting t = 0.34 eV and U = 1.29 eV, the CT bands of **4·5** and **5·5** dimers are calculated at 5480 and 12 760 cm^{-1}, respectively, in agreement with experimental data in Figures 4a and 8. The Hubbard model parameters estimated for **4·5** and **5·5** dimers are fully in line with the standard description of TTF-based dimers[48] and set the stage for the definition of a more complex model accounting for both intermolecular CT and IET in **2·2**, **1·2**, and **1·1** dimers.

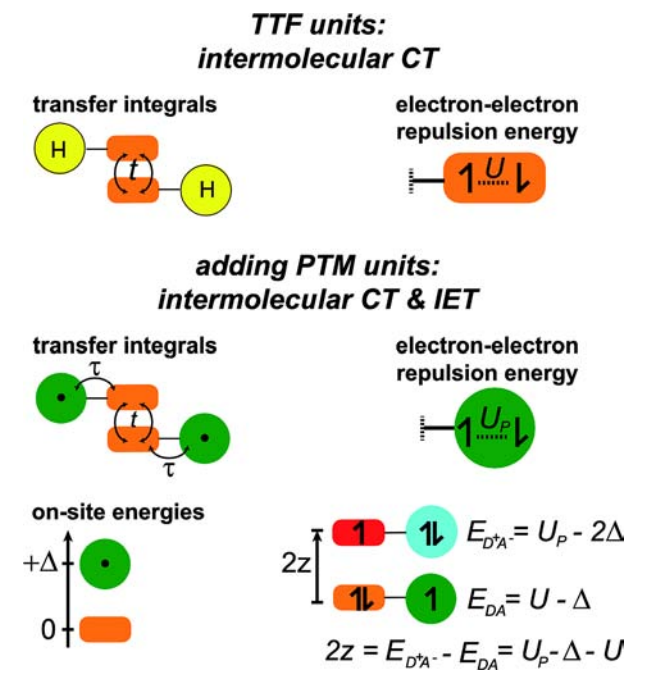

Figure 10. Schematic picture of the model for intermolecular CT and IET.

The IET occurring in dyad **1** can be modeled in terms of the standard two-state model for D−A dyads,[8,10,12] that describes the resonance between a neutral state **1a**, DA (TTF-PTM, in our case), and a zwitterionic state **1b**, D^+A^- (TTF^+·-PTM^-). The relevant Hamiltonian:

$$H_{DA} = 2z|D^+A^-\rangle\langle D^+A^-| - \tau(|DA\rangle\langle D^+A^-| + |D^+A^-\rangle\langle DA|)$$

is defined by two electronic parameters: $2z$, the energy gap between the zwitterionic and the neutral state, and τ, the mixing matrix element. In principle these two parameters can be estimated from the CT absorption of dyad **1**. However, in spite of our efforts, we were not able to observe the relevant absorption peak, due to its intrinsically small intensity and to the low solubility of dyad **1**.

In any case, the basic model for the dimers **2·2**, **1·2**, and **1·1** is a four-site Hubbard model, for a PTM-TTF·TTF-PTM structure, that describes two TTF-PTM molecules, with their typical IET resonance, connected through an intermolecular CT between the paired TTF moieties, as sketched in the lower panel of Figure 10. The parameter Δ measures the energy difference between the TTF and PTM frontier orbitals, and U_P is the repulsion of two electrons residing on the PTM site. The hopping integral between the PTM and TTF moieties is set to the same τ value as for the isolated TTF-PTM dyad **1**. Moreover, in line with chemical intuition and in agreement with the essential state model for D−A dyads, we assume that states with PTM sites bearing a net positive charge are very high in energy so not to contribute to the low-energy physics of the system. To enforce this criterion, we set both U_P and Δ to very large values (as to make their precise value irrelevant), while maintaining their difference finite. In this way only four parameters, $2z = U_P$-Δ-U, τ, t, U are needed to fully define the four state Hubbard model for the **2·2**, **1·2**, and **1·1** dimers, bearing 4, 5, and 6 electrons, respectively. The dimer Hamiltonian can be numerically diagonalized on a real-space basis, as detailed in the SI.

The t and U parameters are transferred from the model for **5·5** and **4·5** dimers, and we set τ = 0.1 eV and $2z$ = 0.45 eV to reproduce the frequency of the CT bands of **2·2** (Figure 4b) and **1·2** (Figure 9). With these parameters the CT transition of the homo dimer **2·2** is calculated at 12 500 cm^{-1}, practically superimposed with the transition of the homo dimer **5·5**, confirming that the intramolecular charge resonance is not important in dyad **2**, where the positively charged TTF units is a poor electron donor. On the other hand, for the MV dimer **1·2** we calculate a first most intense transition at 4230 cm^{-1} and a weaker transition at 5615 cm^{-1}, in line with the observation of a very broad absorption band for the MV dimer **1·2** located at lower energies in comparison with the CT transition observed for the MV dimer **4·5**. This red-shift is a clear indication of the importance of IET in the MV dimer **1·2**. For comparison, the

dx.doi.org/10.1021/ja400281b | J. Am. Chem. Soc. 2013, 135, 6958−6967

CT absorption band of **1** is calculated at 3970 cm^{-1}, but with a very weak intensity (at least 5 times smaller than for all other species discussed above). This intrinsic weakness, associated with the extremely low solubility of **1** in all solvents, hinders the experimental observation of the band. Similarly, the CT absorption for **2** is calculated at 14 230 cm^{-1}, with an extremely low intensity (about 1 order of magnitude smaller than for **1**), again justifying the lack of experimental observation of the relevant band. For this same compound we calculate the triplet-singlet gap around 100 cm^{-1}, suggesting that the species behaves as a biradical at the experimental temperatures.

The four-site model, parametrized against optical spectra of **5·5**, **4·5**, **2·2**, and **1·2**, allows us to address relevant ESR spectra. MV dimer **4·5** is a radical species, in a doublet state, with the unpaired electron equally distributed on the two TTF moieties. The homo dimer **5·5** is more interesting: the calculated triplet-singlet gap Δ_{TS} = 2360 cm^{-1} is much larger than thermal energy, so that **5·5** is found at all temperatures in a pure singlet state and is therefore ESR-silent. In contrast, the singlet−triplet gap Δ_{TS} = 2 cm^{-1} calculated for **2·2** is negligible at all temperatures, proving that **2·2** behaves as a biradical, with the two radicals located at the PTM sites. Quite interestingly, the quintet−singlet gap, Δ_{QS} = 2414 cm^{-1}, is of the same order of magnitude as the triplet−singlet gap for **5·5**, being related to the decoupling of the two electrons responsible for the TTF-TTF supramolecular interaction. In close agreement with experimental data we calculate an antiferromagnetic coupling between the two spins located on the PTM units, driven by the intra- and intermolecular CT interactions: specifically, we calculate a spin−spin correlation function for the spins on the two PTM sites $\langle S_{z1}S_{z4}\rangle$ = −0.249, very close to the theoretical limit of −0.25 for a pure antiferromagnetic interaction.

The MV dimer **1·2** is in a doublet state (S = 1/2), as expected for a free radical. The next spin state (S = 3/2) however lies at 172 cm^{-1}, and is thermally accessible at room temperature suggesting a substantial free-radical character of the spins located at the PTM sites. Even more interesting is the spin distribution on the four sites: the interplay between intra- and intermolecular charge resonance in **1·2** not only causes a broadening and a red-shift of the CT absorption with respect to the **5·5** spectrum, but also affects ESR spectra leading to a redistribution of spin densities in the TTF and PTM sites. Specifically, for the ground state of **1·2** we calculate a ratio between the spin density on the TTF versus PTM site of 0.24, that, in line with the experimental results, is much smaller than the theoretical limit of 0.5 expected for a noninteracting mixture of **1** and **2** molecules in a 1:1 ratio. In the chemically prepared dimer the measured ratio is even smaller (0.1 at room temperature), pointing to a larger contribution of the **1b·2** structure, most probably due to a stabilization of charge-separated structures from environmental effects. This can be mimicked in our model by a decrease of the parameter z. Specifically, setting z = 0 the calculated ratio of TTF vs PTM spin density reduces to 0.16. Quite interestingly, in these conditions the intensity of the CT band becomes negligible in the NIR region, in good agreement with our experiments (cf. Figure S7).

We are now in the position to discuss experimental results for the **1·1** dimer, whose experimental data are discussed in ref 20. Adopting the same parameters as for **2·2** and **1·2** dimers, but putting 6 electrons on the four sites, the most intense CT transition is calculated for **1·1** at 1400 cm^{-1}, well in the mid-IR region. This transition is very difficult to locate experimentally due to its overdamped character (the line width of the CT band is by far larger than its frequency). The second intense transition is located at 6900 cm^{-1}, but its intensity is extremely weak, as to hinder its experimental observation. The calculated singlet−triplet gap is very low (34 cm^{-1}), suggesting that the spins on the PTM units stay unpaired, leading to a recordable ESR signal. We calculate an antiferromagnetic coupling between the two spins with $\langle S_{z1}S_{z4}\rangle$ = −0.174. These results are consistent with the experimental ESR spectra in nonpolar solvents, where the species **1** is in a largely neutral ground state. Indeed in the dimer **1·1** we calculate a charge distribution with 1.16 electrons residing on PTM sites and 1.84 on the TTF sites.

To simulate the behavior of **1·1** dimers in polar solvents, we decrease the $2z$ value, effectively reducing the energy of the zwitterionic state, stabilized by the polar solvent. Setting $2z$ = 0, we obtain a ground state where a sizable fraction of charge is transferred from the TTF to the PTM sites, leading to 1.67 electrons on the PTM sites and 1.33 electrons on the TTF sites. With this charge configuration, the singlet triplet gap is calculated at 583 cm^{-1}, indicating that in polar solvents the dimer **1·1** is found in a singlet state, and is therefore ESR silent, in agreement with experimental results.

SUMMARY AND CONCLUSIONS

This work represents a first exhaustive analysis of complex materials where TTF-units behave both as the donor unit in D−A dyads and as the building block of supramolecular aggregates. The subtle interplay between the IET process within the dyad with the intermolecular CT occurring between the two TTF units in each supramolecular aggregate has been thoroughly investigated via optical and magnetic spectroscopic measurements and is well rationalized by a theoretical model that merges a Hubbard-like description of the intermolecular CT interaction with an essential state description of the IET. The resulting picture suggests that new physics and new materials can emerge by a careful coupling of IET and CT degrees of freedom and TTF-based dyads, which are particularly promising to obtain bistable materials for the design of future molecule-based spin-electronic devices.

ASSOCIATED CONTENT

Supporting Information

Experimental procedures and characterization data; method used to determine the thermodynamic parameters of the different dimerization equilibria and related information; T-dependent ESR and UV/vis/NIR spectra of mixtures of isolated **1** and **2**; details of numerical calculations. This material is available free of charge via the Internet at http://pubs.acs.org.

AUTHOR INFORMATION

Corresponding Author

*E-mail: vecianaj@icmab.es.

Present Addresses

[⊥]Department of New Materials and Biosystems, Max Planck Institute for Intelligent Systems, Heisenbergstr. 3, D-70569 Stuttgart, Germany & Department of Biophysical Chemistry, University of Heidelberg, INF 253, D-69120 Heidelberg, Germany.

[#]Laboratory for Chemistry of Novel Materials, University of Mons, Place du Parc 20, BE-7000 Mons, Belgium.

Notes

The authors declare no competing financial interest.

■ ACKNOWLEDGMENTS

This work was supported by the DGI grant (POMAs (CTQ2010-19501), the Networking Research Center on Bioengineering, Biomaterials, and Nanomedicine (CIBER-BBN), and the Generalitat de Catalunya (grant 2009SGR00516). J. G. is grateful to the Consejo Superior de Investigaciones Científicas (CSIC) for a JAE fellowship and M. S. to the MEC for a FPU predoctoral grant.

■ REFERENCES

(1) Matsushita, M. M.; Kawakami, H.; Sugawara, T. *Phys. Rev. B* **2008**, *77*, 195208.
(2) Prinz, G. A. *Science* **1998**, *282*, 1660.
(3) Johnson, M. *J. Phys. Chem. B* **2005**, *109*, 14278.
(4) Bloom, F. L.; Wagemans, W.; Kemerink, M.; Koopmans, B. *Phys. Rev. Lett.* **2007**, *99*, 257201.
(5) Sugawara, T.; Matsushita, M. M. *J. Mater. Chem.* **2009**, *19*, 1738.
(6) Nishida, S.; Morita, Y.; Fukui, K.; Sato, K.; Shiomi, D.; Takui, T.; Nakasuji, J. *Angew. Chem. Int. Ed.* **2005**, *44*, 7277.
(7) Lehn, J.-M. *Science* **2002**, *295*, 2400.
(8) D'Avino, G.; Grisanti, L.; Guasch, J.; Ratera, I.; Veciana, J.; Painelli, A. *J. Am. Chem. Soc.* **2008**, *130*, 12064.
(9) D'Avino, G.; Grisanti, L.; Painelli, A.; Guasch, J.; Ratera, I.; Veciana, J. *CrystEngComm* **2009**, *11*, 2040.
(10) Grisanti, L.; D'Avino, G.; Painelli, A.; Guasch, J.; Ratera, I.; Veciana, J. *J. Phys. Chem. B* **2009**, *113*, 4718.
(11) Freo, L. D.; Terenziani, F.; Painelli, A. *J. Chem. Phys.* **2002**, *116*, 755.
(12) Terenziani, F.; D'Avino, G.; Painelli, A. *ChemPhysChem* **2007**, *8*, 2433.
(13) Hasegawaa, M.; Iyoda, M. *Chem. Soc. Rev.* **2010**, *39*, 2420.
(14) Bejger, C.; Park, J. S.; Silvera, E. S.; Sessler, J. L. *Chem. Commun.* **2010**, *46*, 7745.
(15) Ziganshina, A. Y.; Ko, Y. H.; Jeon, W. S.; Kim, K. *Chem. Commun.* **2004**, 806.
(16) Williams, J. M.; Ferraro, J. R.; Thorn, R. J.; Carlson, K. D.; Geiser, U.; Wang, H. H.; Kini, A. M.; Whangbo, M. H. *Organic Superconductors (Including Fullerenes)*; Prentice-Hall: Englewoods Cliffs, NJ, 1992.
(17) *TTF Chemistry: Fundamentals and Applications of Tetrathiafulvalene*; Kodansha Springer: Berlin, 2004.
(18) Morita, Y.; Suzuki, S.; Sato, K.; Takui, T. *Nat. Chem.* **2011**, *3*, 197.
(19) Rosokha, S. V.; Kochi, J. K. *J. Am. Chem. Soc.* **2007**, *129*, 828.
(20) Guasch, J.; Grisanti, L.; Lloveras, V.; Vidal-Gancedo, J.; Souto, M.; Morales, D. C.; Vilaseca, M.; Sissa, C.; Painelli, A.; Ratera, I.; Rovira, C.; Veciana, J. *Angew. Chem. Int. Ed.* **2012**, *51*, 11024.
(21) Ito, A.; Hata, K.; Kawamoto, K.; Hirao, Y.; Tanaka, K.; Shiro, M.; Furukawa, K.; Kato, T. *Chem.—Eur. J.* **2010**, *16*, 10866.
(22) Coronado, E.; Epstein, A. J. *J. Mater. Chem.* **2009**, *19*, 1670.
(23) Szulczewski, G.; Sanvito, S.; Coey, M. *Nat. Mater.* **2009**, *8*, 693.
(24) Matsushita, M. M.; Kawakami, H.; Sugawara, T.; Ogata, M. *Phys. Rev. B* **2007**, *77*, 195208.
(25) Rovira, C.; Ruiz-Molina, D.; Elsner, O.; Vidal-Gancedo, J.; Bonvoisin, J.; Launay, J.-P.; Veciana, J. *Chem.—Eur. J.* **2001**, *7*, 240.
(26) Green, D. C. *J. Org. Chem.* **1979**, *44*, 1476.
(27) Spanggaard, H.; Prehn, J.; Nielsen, M. B.; Levillain, E.; Allain, M.; Becher, J. *J. Am. Chem. Soc.* **2000**, *122*, 9486.
(28) Park, J. S.; Karnas, E.; Ohkubo, K.; Chen, P.; Kadish, K. M.; Fukuzumi, S.; Bielawski, C. W.; Hudnall, T. W.; Lynch, V. M.; Sessler, J. L. *Science* **2010**, *329*, 1324.
(29) Perepichka, D. F.; Bryce, M. R.; Batsanov, A. S.; Howard, J. A. K.; Cuello, A. O.; Gray, M.; Rotello, V. M. *J. Org. Chem.* **2001**, *66*, 4517.
(30) Bryce, M. R. *J. Mater. Chem.* **2000**, *10*, 589.
(31) Bryce, M. R. *Adv. Mater.* **1999**, *11*, 11.
(32) Rovira, C.; Veciana, J.; Santaló, N.; Tarrés, J.; Cirujeda, J.; Molins, E.; Llorca, J.; Espinosa, E. *J. Organomet. Chem.* **1994**, *59*, 3307.
(33) Lloveras, V.; Vidal-Gancedo, J.; Figueira-Duarte, T. M.; Nierengarten, J.-F.; Novoa, J. J.; Mota, F.; Ventosa, N.; Rovira, C.; Veciana, J. *J. Am. Chem. Soc.* **2011**, *133*, 5818.
(34) Spruell, J. M.; Coskun, A.; Friedman, D. C.; Forgan, R. S.; Sarjeant, A. A.; Trabolsi, A.; Fahrenbach, A. C.; Barin, G.; Paxton, W. F.; Dey, S. K.; Olson, M. A.; Benítez, D.; Tkatchouk, E.; Colvin, M. T.; Carmielli, R.; Caldwell, S. T.; Rosair, G. M.; Hewage, S. G.; Duclairoir, F.; Seymour, J. L.; Slawin, A. M. Z.; Goddard, W. A.; Wasielewski, M. R.; Cooke, G.; Stoddart, J. F. *Nat. Chem.* **2010**, *2*, 870.
(35) Benz, M. E.; Tabakovic, I.; Miller, L. L. *Chem. Mater.* **1994**, *6*, 351.
(36) Khodorkovsky, V.; Shapiro, L.; Krief, P.; Shames, A.; Mabon, G.; Gorgues, A.; Giffard, M. *Chem. Commun.* **2001**, 2736.
(37) Chiang, P.-T.; Chen, N.-C.; Lai, C.-C.; Chiu, S.-H. *Chem.—Eur. J.* **2008**, *14*, 6546.
(38) Garcia-Yoldi, I.; Miller, J. S.; Novoa, J. J. *J. Phys. Chem. A* **2009**, *113*, 484.
(39) Halling, M. D.; Bell, J. D.; Pugmire, R. J.; Grant, D. M.; Miller, J. S. *J. Phys. Chem. A* **2010**, *114*, 6622.
(40) Bryce, M. R. *Chem. Soc. Rev.* **1991**, *20*, 355.
(41) Huchet, L.; Akoudad, S.; Levillain, E.; Roncali, J.; Emge, A.; Baüerle, P. *J. Phys. Chem. B* **1998**, *102*, 7776.
(42) Tanaka, K.; Ishiguro, F.; Chujo, Y. *Langmuir* **2010**, *26*, 1152.
(43) Levillain, E.; Roncali, J. *J. Am. Chem. Soc.* **1999**, *121*, 8760.
(44) Yoshizawa, M.; Kumazawa, K.; Fujita, M. *J. Am. Chem. Soc.* **2005**, *127*, 13456.
(45) Hasegawa, M.; Takano, J.-I.; Enozawa, H.; Kuwatani, Y.; Iyoda, M. *Tetrahedron Lett.* **2004**, *45*, 4109.
(46) Iyoda, M.; Hasegawaa, M.; Kuwatani, Y.; Nishikawa, H.; Fukami, K.; Nagase, S.; Yamamoto, G. *Chem. Lett.* **2001**, *11*, 1146.
(47) Lyskawa, J.; Sallé, M.; Balandier, J.-Y.; Derf, F. L.; Levillain, E.; Allain, M.; Viel, P.; Palacin, S. *Chem. Commun.* **2006**, 2233.
(48) Torrance, J. B.; Scott, B. A.; Welber, B.; Kaufman, F. K.; Seiden, P. E. *Phys. Rev. B* **1979**, *19*, 730.

■ NOTE ADDED AFTER ASAP PUBLICATION

The Abstract was incorrect in the version published ASAP on April 22, 2013. The corrected version was re-posted on April 24, 2013.